JOURNAL OF GEOPHYSICAL RESEARCH, VOL. 104, NO. D23, PAGES 30,417–30,426, DECEMBER 20, 1999

Fully equivalent operational models for atmospheric chemical kinetics within global chemistry-transport models

S. W. Wang,[1] H. Levy II,[2] G. Li,[3] and H. Rabitz[3]

Abstract. A major portion of the computational effort in simulations by three-dimensional (3-D) chemistry-transport models is consumed in chemical kinetics calculations which repeatedly solve coupled ordinary differential equations. To address this burden, this paper introduces a high-speed fully equivalent operational model (FEOM) for chemical kinetics calculations. The FEOM consists of a hierarchical correlated-function expansion capturing the input-output relationships of chemical kinetics. As an initial test of the FEOM approach for chemical kinetics calculations in 3-D models, this paper develops the FEOMs for CO-CH_4-NO_y-H_2O chemistry to obtain the time-dependent chemical ozone production and destruction rates in global chemistry-transport model (GCTM) simulations. The FEOMs are constructed for all GCTM model levels, all 12 months of the year, every 10° of latitude, for two types of surface albedo, and for all tropospheric values of H_2O, CO, NO_x, and O_3. It is shown that the simulated global ozone fields using the FEOMs in the GCTM ozone simulation are at least as accurate and in some cases better than those obtained by using four-dimensional interpolative look-up tables. Future work will expand the FEOM approach to more detailed chemical schemes, including nonmethane hydrocarbon chemistry in 3-D chemistry-transport model simulations.

1. Introduction

Chemical kinetics calculations are often the most computationally intensive components of three-dimensional (3-D) atmospheric chemistry-transport simulations. Typically, integration of the chemistry rate equations consumes as much as 90% of the total CPU time. This computational burden arises from the chemistry rate equations being nonlinear, highly coupled, and stiff, such that they require the use of elaborate numerical integration schemes (e.g., the Gear-type implicit solvers). This situation will become more severe as additional chemical species and reactions are included.

To circumvent this computational difficulty, parameterized polynomial expansions or interpolative look-up tables have been introduced to fit the integration results of chemistry rate equations "off line" and then employed in 3-D calculations for the chemical kinetics component [e.g., *Klonecki and Levy*, 1997; *Turanyi*, 1994; *Spivakovsky et al*., 1990a]. One major problem associated with these approaches is that without the possibility of simplification the number of times of integrating chemistry rate equations (hereinafter called the sampling effort) needed to obtain the fits grows exponentially with respect to the dimension of the chemical system (i.e., the number of input variables). This comment may be understood from consideration of the effort required to deduce the chemical kinetic input-output mapping by sampling with s points in each of the n input variables (e.g., initial chemical species concentrations) corresponding to the computational cost scaling as $\sim s^n$. Realistically, one may expect s to be $10 \sim 20$ and n to be $10 \sim 10^2$ or larger in typical chemical systems. Furthermore, the evaluation of a new point by interpolation in an n-dimensional space for $n \gg 1$ would be exceedingly difficult with an interpolative look-up table. Therefore the attempts to pursue these traditional approaches would be prohibitive in high-dimensional chemical systems.

This paper presents an alternative to the above approaches by creating fully equivalent operational models (FEOMs) for the chemical kinetics. A FEOM is an expansion of correlated functions with increasing dimension which capture the chemical kinetic input-output relationships. In this fashion the original high-dimensional interpolation problem is broken into a set of low-dimensional pieces which may be efficiently handled. From these quantitative input-output relationships, the FEOM can be used to directly calculate output species chemical tendencies (chemical production rates minus chemical destruction rates) and related chemical properties based on the initial input species concentrations. It has been shown that the FEOM technique can produce accurate chemical species concentrations, while being orders of magnitude faster than a conventional stiff equation solver in a photochemical box-model study of 46 input variables [*Shorter et al*., 1999]. The main focus of this paper is to extend the application of the FEOM technique for chemical kinetic calculations to a 3-D global chemistry transport model (GCTM) study, where the dynamic ranges of the chemical species concentrations are far broader than in the previous photochemical box model study [*Shorter et al*., 1999].

As an initial test for the FEOM technique in 3-D global scale models, we will construct the FEOMs for the chemistry of the CO-CH_4-NO_y-H_2O system to obtain the time-dependent chemical ozone production and destruction rates in a GCTM ozone simulation. The structure of this paper is as follows:

[1]Atmospheric and Oceanic Sciences Program, Princeton University, Princeton, New Jersey.
[2]Geophysical Fluid Dynamics Laboratory, Princeton, New Jersey.
[3]Department of Chemistry, Princeton University, Princeton, New Jersey.

Paper number 1999JD900830.
0148-0227/99/1999JD900830$09.00

Section 2 describes the technique for creating the FEOMs. The process of generating the FEOMs for the CO-CH_4-NO_y-H_2O chemistry is presented in section 3. The incorporation of the FEOMs into the 3-D GCTM simulation is shown in section 4. Some brief conclusions are given in section 5.

2. Methodology: Fully Equivalent Operational Models (FEOMs)

The major difficulty in mapping the input-output relationship of high-dimensional complex systems comes from the apparent exponentially large sampling effort when using the traditional approaches, as mentioned earlier. This problem can be resolved by the FEOM technique, which is a systematic mapping procedure between sets of input and output variables. The FEOM technique is a special application of a family of high-dimensional model representation tools [*Rabitz et al*., 1998; *Rabitz and Alis*, 1999]. The representation of the high-dimensional FEOM map of the input variables $\mathbf{x} = (x_1, x_2, \cdots, x_n)$ upon an output $g(\mathbf{x})$ is exactly expressed as an expansion of hierarchical correlated functions $f_0, f_i(x_i), f_{ij}(x_i, x_j)$, etc., as follows:

$$g(\mathbf{x}) = f_0 + \sum_{i=1}^{n} f_i(x_i) + \sum_{1\le i<j\le n} f_{ij}(x_i, x_j) + \sum_{1\le i<j<k\le n} f_{ijk}(x_i, x_j, x_k) + \cdots + f_{12\cdots n}(x_1, x_2, \cdots, x_n). \quad (1)$$

Here f_0 denotes the mean effect, which is a constant. The function $f_i(x_i)$ is a first-order term giving the effect associated with the variable x_i acting independently, although generally nonlinearly, upon the output $g(\mathbf{x})$. The function $f_{ij}(x_i, x_j)$ is a second-order term describing the cooperative effects of the variables x_i and x_j upon the output $g(\mathbf{x})$. The higher-order terms reflect the cooperative effects of increasing numbers of input variables acting together to influence the output $g(\mathbf{x})$. The last term $f_{12\cdots n}(x_1, x_2, \cdots, x_n)$ gives any residual dependence of all the input variables locked together in a cooperative way to influence the output $g(\mathbf{x})$. It is important to note that the full FEOM expansion is of finite order, and it is by definition an exact representation of the output variable $g(\mathbf{x})$.

The FEOM expansion is a very efficient formulation for high-dimensional mapping in complex systems if the higher-order variable correlations are weak, thereby permitting the input-output relationship behavior to be captured by the terms of low-order l with $l \ll n$. The computational effort to determine the expansion functions using the cut method (see below) will scale polynomically with n rather than exponentially. This logic is based on the fundamental assumption underlying the FEOM representation that only low-order correlations among the input variables will probably have significant impacts upon the outputs for most high-dimensional complex systems. Various studies [*Rabitz et al*., 1998; *Rabitz and Alis*, 1999; *Shim and Rabitz*, 1998; *Rabitz and Shim*, 1999; *Shorter et al*., 1999] verify this rapid convergence behavior of the FEOM expansion. With this property, the FEOM technique provides a powerful tool for mapping the input-output relationship behavior in complex systems.

The key to utilizing the FEOM technique is the ability to compute rapidly the expansion terms shown in (1). There are various means to determine the FEOM expansion functions with different levels of effort, and the choice among these methods depends on the system dimension, the ability to sample the input and other factors. In this paper, a cut-FEOM procedure will be employed. With the cut FEOM, a reference point $\bar{\mathbf{x}} = (\bar{x}_1, \bar{x}_2, \cdots, \bar{x}_n)$ is defined in the variable space, and the expansion functions are determined by evaluating the input-output responses of the system relative to the defined reference point $\bar{\mathbf{x}}$ along associated lines, surfaces, subvolumes, etc. (i.e., cuts), in the input variable space. This process is described as follows:

$$f_0 = g(\bar{\mathbf{x}}), \quad (2)$$

$$f_i(x_i) = g(x_i, \bar{\mathbf{x}}^i) - f_0 = g(x_i, \bar{\mathbf{x}}^i) - g(\bar{\mathbf{x}}), \quad (3)$$

$$f_{ij}(x_i, x_j) = g(x_i, x_j, \bar{\mathbf{x}}^{ij}) - f_i(x_i) - f_j(x_j) - f_0, = g(x_i, x_j, \bar{\mathbf{x}}^{ij}) - g(x_i, \bar{\mathbf{x}}^i) - g(x_j, \bar{\mathbf{x}}^j) + g(\bar{\mathbf{x}}), \cdots, \quad (4)$$

where the terminology $g(x_i, \bar{\mathbf{x}}^i) \equiv g(\bar{x}_1, \bar{x}_2, \cdots, \bar{x}_{i-1}, x_i, \bar{x}_{i+1}, \cdots, \bar{x}_n)$ means that all the input variables are at the reference point values except x_i, etc. The f_0 term is the output response of the system evaluated at the reference point $\bar{x}$. The higher-order terms are evaluated as cuts in the input variable space through the reference point. Therefore each first-order term $f_i(x_i)$ is evaluated along its variable axis through the reference point. Each second-order term $f_{ij}(x_i, x_j)$ is evaluated in a plane defined by each binary set of input variables through the reference point, etc. The process of subtracting off the lower-order expansion functions removes their dependence to assure a unique contribution from the new expansion function. Thus the expansion functions only contain information of the specified level of interaction, and they satisfy the following orthogonality conditions [*Rabitz et al*., 1998]:

$$f_{ij\cdots l}(x_i, x_j, \cdots, x_l)|_{x_s=\bar{x}_s} = 0, \quad \text{for } s \in (i, j, \cdots, l). \quad (5)$$

This property permits the independent sequential evaluations of the FEOM functions.

In practice, each of the FEOM expansion functions is numerically represented as a low-dimensional look-up table over its variables. Note that by virtue of (5), the FEOM in (1) is exact along any of the cuts. Then, the output response $g(\mathbf{x})$ at a point $\mathbf{x}$ off the cuts can be obtained by the following procedure: (1) interpolate each of the FEOM expansion terms in the look-up tables with respect to the input values of the point $\mathbf{x}$ and (2) sum the interpolated values of the FEOM terms from zeroth order to the highest order retained in keeping with the desired accuracy. Because of the rapid convergence behavior of the FEOM expansion and its need for only low-dimensional look-up tables, the original problem of high-dimensional input-output mapping is resolved. The breakdown of the input-output map into a distinct set of orthogonal low-dimensional components is a primary distinction of FEOM from other traditional fitting techniques such as the least squares fitting. Importantly, a large number of the FEOM expansion functions may be insignificant relative to the f_0 term. These functions can be identified and eliminated from the FEOM expansion by selectively sampling each function to determine its magnitude, such that a more concise FEOM expansion can be generated.

A specific application of the FEOM expansion is to provide an efficient means for replacing very time consuming modeling

processes with an equivalent input-output relationship. For example, the process of integrating chemical rate equations in 3-D chemistry-transport model simulations consumes the major portion of the total CPU time. Instead of repeatedly integrating the chemistry rate equations, we can construct a FEOM to approximate all of the chemical kinetic input-output relationships and employ them in the 3-D model simulations. The benefit of the FEOM approach is that after an initial investment of computational effort, the equivalent model output can be obtained with a relatively small amount of computing time. In this paper, we illustrate the use of FEOMs for chemical kinetics calculations for the nonlinear tropospheric ozone mechanism involving CO-CH_4-NO_y-H_2O and the incorporation of these FEOMs into a GCTM study.

3. FEOMs for CO-CH_4-NO_y-H_2O Chemistry

The purpose of building the FEOM is to capture the input-output behavior of chemical kinetics through the observation of a series of photochemical box-model runs which integrate the chemical rate equations. A zero-dimensional photochemical box model, which utilizes the standard CO-CH_4-NO_y-H_2O chemical mechanism [*Klonecki and Levy*, 1997] and the standard acetone mechanism [*McKeen et al*., 1997; *Klonecki*, 1998], was used to calculate the chemical ozone production and destruction rates for incorporation into the 3-D GCTM ozone simulation. The rates of the photodissociation reactions in the mechanisms are calculated with a radiative-transfer model [*Perliski*, 1992; *Meier et al*., 1982] which includes the effect of ground albedo and multiple Rayleigh scattering. The radiative transfer model takes as input the observed temperature profiles [*Barnett and Corney*, 1985] and a merged ozone data set [*Orris*, 1997; *Logan*, 1985; *Komhyr et al*., 1989; *Spivakovsky et al*., 1990b; *Keating et al*., 1990]. The rates of the remaining reactions were calculated using the recommended values from *DeMore et al*. [1994].

The CO-CH_4 mechanism has 22 species, four of which are held at constant mixing ratios: CH_4, H_2, O_2, and HNO_3. The first three represent well-mixed species in the troposphere. HNO_3 is held at a constant mixing ratio because its two main sinks are deposition and wet removal, and it is not generally in photochemical steady state with NO_x. Moreover, nitric acid at concentrations observed in the troposphere does not affect the net photochemical rates of change of ozone (hereinafter called the chemical ozone tendencies) in a significant way. The details of this photochemical box model are presented by *Klonecki and Levy* [1997].

To conform with the diurnally averaged radiation assumption used to generate the meteorological fields in the 3-D GCTM ozone simulation, the system of rate equations in the box model was integrated in time through a number of diurnal cycles until a diurnal steady state is achieved. Thus each box-model run produced the outputs of the diurnally averaged ozone chemical production and destruction rates based on the given inputs: time of the year (month), location (altitude, latitude, over land or sea), and specification of the tracer species (O_3, NO_x, CO, and H_2O) concentrations that can influence the chemical rates of production and destruction of ozone.

To meet the requirements of the 3-D GCTM, box model runs were carried out for a number of mixing ratios that covered the tropospheric ranges of O_3, NO_x, CO, and H_2O at 17 latitudes, seven altitudes, 12 months, and two types of albedo surfaces (land and sea). At the first stage of the FEOM development we tried to incorporate all of the input variables into the FEOM expansion up to second order. However, the FEOM constructed to this order could not provide sufficient accuracy for predicting chemical ozone production and destruction rates. Without reconstructing to a higher-order FEOM, a more sophisticated means, we found that the second-order FEOMs constructed by the four input variables (mixing ratios of O_3, CO, NO_x, and H_2O) had good accuracy. Therefore the FEOMs constructed by these four variables are generated for each of the 3-D GCTM grid boxes to perform the chemical kinetics calculations in every model time step.

Table 1. Grid Resolution of Large-Scale FEOMs

Input Variable	Range	Reference Point
Relative humidity	10%, 20%, 30%, $\cdots$, 90%, 100%	50%
CO, ppb	20, 40, 60, $\cdots$, 180, 200	100
NO_x, ppt	1, 50, 100, $\cdots$, 900, 950	450
Ozone, ppb	10, 20, 30, $\cdots$, 190, 200	100

FEOM, fully equivalent operational model.

We select the midpoint in each of the four dynamic ranges of input variables (mixing ratios of O_3, CO, NO_x, and H_2O) as the reference point $\bar{x}$ in (2)–(4) to construct a FEOM at a given latitude, altitude, month, and surface type. Two FEOM expansions, corresponding to the outputs of the diurnally averaged chemical ozone production and destruction rates, were evaluated relative to this reference point. Within the four specified dynamic ranges of input variables, the sampling grid points were taken from the equally spaced intervals along each input variable axis tabulated in Table 1.

According to the formulas specified in (2)–(4) the individual FEOM expansion terms were obtained by algebraic manipulations of the box-model outputs. Special care is necessary to ensure that the relevant portion of the input variable space is covered by the chosen sampling points for the box-model runs. The calculated FEOM expansion terms from zeroth order to the highest desired order (second order in the present paper) were saved as look-up tables with respect to the chosen sampling points. Thus the output $g(\mathbf{x})$ evaluated at a point $\mathbf{x}$ off those sampling points can be obtained by interpolation and algebraic manipulation of the FEOM tables. The goal is to employ the FEOMs for calculating diurnally averaged ozone production and destruction rates for each grid box of the model troposphere at every time step in the 3-D GCTM ozone simulation.

3.1. Off-Line Testing of FEOMs

To determine the highest desired order of the FEOM expansion, "off-line" testing of the FEOM predictions was performed. First, we calculated the FEOM expansion up to second order to test if it can capture the essential relationships between the four input variables and two output variables. Then, we compared the FEOM predictions of chemical ozone production and destruction rates with those obtained from box-model runs for the complete set of uniformly sampled points in the four-dimensional input variable space to ensure the convergence of the FEOM expansion. By multiplying the numbers of grid points along each input variable axis specified in Table 1 ($10(H_2O) \times 10(CO) \times 20(NO_x) \times 20(O_3)$, a complete sampling effort would call for 40,000 box-model runs for a given latitude, altitude, month, and surface type.

Table 2. Relative Errors of FEOM Predictions

Latitude	Relative Error (RE)	O_3 Production*	O_3 Destruction*
−49.5°	5%	67%	81%
	10%	81%	89%
	20%	91%	94%
−1.5°	5%	90%	92%
	10%	96%	96%
	20%	99%	98%
49.5°	5%	87%	89%
	10%	94%	95%
	20%	98%	98%

*Percent of test runs lying within the stated relative error (RE).

The number of box-model runs required to determine the FEOM expansion depends on the number of input variables and the number of sampling grid points for each input variable. If s_i grid points are used for the ith input variable, then $s_i - 1$ box-model runs are required to specify the ith first-order expansion term $f_i(x_i)$. The model run at the reference point is not required since the value of the first-order expansion is zero at that point by virtue of (3) and (5). In an analogous manner, $(s_i - 1)(s_j - 1)$ model runs are required to determine each second-order term $f_{ij}(x_i, x_j)$. In the present case there is one f_0 term, 4 f_i terms (f_1, f_2, f_3, f_4), and 6 f_{ij} terms (f_{12}, f_{13}, f_{14}, f_{23}, f_{24}, f_{34}) determined for the FEOM up to second order. Therefore a total of 1183 box-model runs are required to construct a FEOM by summing up the numbers of box model runs as follows: $1(f_0) + 9(f_1) + 9(f_2) + 19(f_3) + 19(f_4) + 9 \times 9(f_{12}) + 9 \times 19(f_{13}) + 9 \times 19(f_{14}) + 9 \times 19(f_{23}) + 9 \times 19(f_{24}) + 19 \times 19(f_{34})$. Compared to a full resolution complete sampling of 40,000 mentioned above, the FEOM only calls for 3% of that effort to second order.

To use the constructed FEOM in the 3-D GCTM ozone simulation, 2856 FEOMs need to be constructed to account for all the combinations of 17 latitudes (from 80°S to 80°N with 10° resolution), seven pressure levels (990, 940, 835, 685, 500, 315, and 190 mbar), 12 months, and two types of surface albedo (land and sea). We present the general quality of the "off-line" testing for these FEOMs at three different latitudes at the surface level (990 mbar) in a specific month (July) over land. The behavior found in this test is typical of the overall results under other conditions. The comparisons are between ozone production and destruction rates obtained from box model runs and the FEOM predictions conducted over the 40,000 complete grid points in the four-dimensional input variable space. Denoting f_t as a predicted value from the FEOM, and f_r as the box model output value, then we define the relative error (RE) as follows:

$$\mathrm{RE} = \left| \frac{f_t - f_r}{f_r} \right|. \quad (6)$$

Table 3. Absolute Errors of FEOM Predictions at Latitude = −49.5

Absolute Error (AE)	O_3 Production*	O_3 Destruction*
0.05 ppb/d	93%	99%
0.1 ppb/d	99%	100%
0.2 ppb/d	100%	100%

*Percent of test runs lying within the stated absolute error (AE).

We present the quality of the FEOM predictions by calculating the percentages of the total 40,000 points, which are within a RE of 5, 10, and 20%, respectively.

According to the results shown in Table 2, good agreement between the FEOM predictions and the box-model outputs are shown at the areas around the tropics and the midlatitudes in the Northern Hemisphere, since almost 90% of the complete sampling points are within 5% RE. Weaker agreement is found in the area around the midlatitudes in the Southern Hemisphere; this errant behavior is misleading as it arises from the fact that the magnitudes of the box-model outputs are very small (i.e., the denominator in (6) is very small), such that a small deviation in the FEOM predictions can cause a large offset in the relative errors.

Following up upon the latter comments, the sensitivity study by *Klonecki and Levy* [1997] shows that the magnitudes of the chemical ozone production and destruction rates are much lower in winter than in summer. This explains the offset of the REs seen in the midlatitude of the Southern Hemisphere, since it is winter there in the month of July. Under such conditions the quality of the FEOM predictions can be demonstrated from the absolute errors (AEs) as shown in Table 3 at latitude −49.5°.

From the results shown in Tables 2 and 3 the deviations between the FEOM predictions and the box-model outputs are very small. These off-line testing results confirm the effective convergence of the second-order FEOM, which will be used in the 3-D GCTM ozone simulations.

Before the incorporation of the FEOMs into the GCTM simulation, special care was paid to examining the ranges of the 3-D fields of the four input variables (NO_x, CO, H_2O, and O_3), to ensure that the relevant portions of the four-dimensional input variable space were properly covered by the constructed FEOMs. Strong variations in NO_x and O_3 concentration fields are found across the different types of surface albedo (land or sea) at the regions near the tropics and subtropics in the lower troposphere. In the ocean part of these areas the NO_x and O_3 concentrations are often very low ($NO_x < 10$ ppt, $O_3 < 10$ ppb), compared to those fields in the land part ($NO_x > 200$ ppt, $O_3 > 50$ ppb). Thus the large-scale FEOMs using the grid resolutions and the reference point specified in Table 1 may not capture the input-output relationships well in the ocean part of these regions, since the input values of NO_x and O_3 concentrations are falling far away from the reference point values of $NO_x = 450$ ppt, $O_3 = 100$ ppb (i.e., their cut center values). Therefore a set of small-scale FEOMs were constructed separately by moving the reference point values (i.e., the cut center) of the NO_x and O_3 concentrations to lower values. The specified ranges of the four input variables and the reference point for these small-scale FEOMs are shown in Table 4.

Table 4. Ranges of Four Input Variables for Small-Scale FEOMs

Input Variable	Range	Reference Point
Relative humidity	20%, 60%, 100%	60%
CO, ppb	50, 75, 100	75
NO_x, ppt	1, 5, 10, 15, 20	10
Ozone, ppb	1, 5, 10, 15, 20	10

4. The 3-D GCTM Ozone Simulation

There are four major components controlling tropospheric O_3 concentrations in this GCTM ozone simulation: (1) transport of ozone from the stratosphere, (2) chemical production and destruction due to the CO-CH_4-NO_y-H_2O chemistry in the clean troposphere, (3) chemical production in the polluted continental boundary layer in the presence of reactive hydrocarbons, and (4) dry deposition at the surface. In a previous GCTM ozone simulation [*Levy et al*., 1997] the chemical ozone production and destruction rates due to CO-CH_4-NO_y-H_2O chemistry were obtained by interpolating four-way look-up tables with respect to the inputs of four tracer concentrations (O_3, NO_x, CO, and H_2O) at every GCTM model time step [*Klonecki and Levy*, 1997]. As a test, the FEOMs are used to obtain the chemical ozone production and destruction rates in the GCTM simulation in place of the four-way look-up tables. The other three model components remained the same as in the previous simulation [*Levy et al*., 1997].

The GCTM has a horizontal resolution of ~265 km, 11 terrain following "sigma" levels in the vertical direction at standard pressures of 10, 38, 65, 110, 190, 315, 500, 685, 835, 940, and 990 mbar, and it is driven by 12 months of 6-hour time-averaged wind, temperature, and precipitation fields from a general circulation model (GCM) [*Manabe et al*., 1974]. The GCM was run with 24-hour-averaged solar insolation, therefore the GCTM cannot realistically simulate transport processes dependent on the diurnal cycle. This is the main reason why we calculated the diurnally averaged rates of chemical ozone production and destruction in the box-model runs mentioned in the previous section. The details of the GCTM are described by *Mahlman and Moxim* [1978], *Levy et al*. [1982], *Levy and Moxim* [1989], and *Kasibhatla et al*. [1993].

4.1. GCTM Simulation With FEOMs

Since O_3 is the only tracer in this GCTM ozone simulation, the concentration fields of the other three tracers were prepared prior to the current ozone simulation. The fields of the H_2O concentrations were obtained from the monthly averages of observation data. The CO fields were taken from 6-hour averages of carbon monoxide GCTM simulations of *Kasibhatla et al*. [1996] and T. Holloway et al. (Global distribution of carbon monoxide, submitted to *Journal of Geophysical Research*, 1999), and the fields compare well with the observed surface values. The NO_x fields were obtained from a GCTM NO_x simulation, described by *Kasibhatla et al*. [1993], *Moxim et al*. [1996], *Levy et al*. [1996], and captured the observed behavior [*Levy et al*., 1999]. The NO_x and CO GCTM simulations were run with the same meteorological conditions (i.e., winds, surface pressure, precipitation) as the current ozone simulation.

With the incorporation of large- and small-scale FEOMs into the GCTM the simulated global ozone fields are compared with those obtained from the previous simulation [*Levy et al*., 1997] using the four-way look-up tables. These two sets of global ozone fields are compared by calculating the ratios of the ozone concentrations in each of the GCTM grid boxes, and then these ratios are plotted in each grid box throughout the model troposphere. The monthly averaged ratios for July at two pressure levels (190 and 500 mbar) and 1σ level (sigma = 0.990) are shown in Figure 1, since the agreement patterns in the upper, middle, and lower troposphere are represented by these three levels.

Table 5. Comparisons of Chemical Ozone Tendencies (ppb/d)

Grid Box	H_2O	CO, ppb	NO_x, ppt	O_3, ppb	AAK*	FEOM	Exact Solution
1	90%	63.6	3.5	5.1	−0.58	−0.73	−0.66
2	90%	63.5	2.0	5.1	−0.70	−0.83	−0.81
3	90%	64.3	2.4	5.5	−0.74	−0.87	−0.83

*AAK refers to the four-way look-up table.

From the results shown in Figure 1 the ratios are generally between 0.9 and 1.1 (i.e., within 10% error) across all levels of the troposphere. The higher disagreements (from 5 to 10%) appear in regions of the middle and lower troposphere. These higher disagreements are due to the differences between the chemical ozone tendencies obtained from the FEOMs and the four-way look-up tables. We selected three grid boxes in the lowest tropospheric level (sigma = 0.990) over the Pacific Ocean at the latitude of 15°N, where the worst disagreement is appearing, to reveal the differences of the chemical ozone tendencies obtained from these two methods. In order to judge the correctness of the chemical ozone tendencies predicted by these two methods, we also extracted the values of four input variables (the mixing ratios of O_3, NO_x, CO, and H_2O) in these three grid boxes to obtain the numerically exact solutions of chemical ozone tendencies by performing box-model runs. The comparisons are shown in Table 5.

From the results shown in Table 5 the FEOM predictions produce more accurate chemical ozone tendencies than those obtained from the four-way look-up tables. Also, the percentage differences between the chemical ozone tendencies obtained from these two methods explain the disagreements seen in the comparisons of the simulated ozone fields in section 4.3. The prediction offsets using the four-way look-up tables arise from an accumulation of interpolation errors in the four-dimensional input variable space. The FEOM interpolation is more easily and accurately performed, as at most, it involves two-dimensional variable subspaces with the second-order FEOM.

4.2. Evolution of FEOM Resolutions

To perform 1-year GCTM ozone simulations, 2856 sets of large and small FEOMs are needed. Each of the large FEOMs requires 1183 box-model runs based on the fine sampling resolutions specified in Table 1, while each of the small FEOMs only requires 65 box-model runs due to the much smaller number of the sampling grid points specified in Table 4. The total computational overhead to construct the large FEOMs calls for performing ~3.4 million box-model runs.

These efforts can be reduced at little loss of accuracy, if the sampling grid resolution is made more coarse. After trying a series of different combinations of grid resolutions, the coarse scale grid resolutions for constructing the new large FEOMs are chosen as shown in Table 6. The number of grid points for the coarse resolution FEOM shown in Table 6 are 3 (H_2O), 3 (CO), 20 (NO_x), and 10 (O_3), respectively. The grid resolution of the NO_x variable remained the same as in the finer scale, and the resolution of the O_3 variable was reduced by a factor of 2. Chemical ozone production and destruction rates are very sensitive to variations in NO_x and O_3 values [*Klonecki and Levy*, 1997], and these finer resolutions were deemed appropriate. The resolution of the other two variables (H_2O and CO) were greatly reduced, approximately by a factor of 3, since

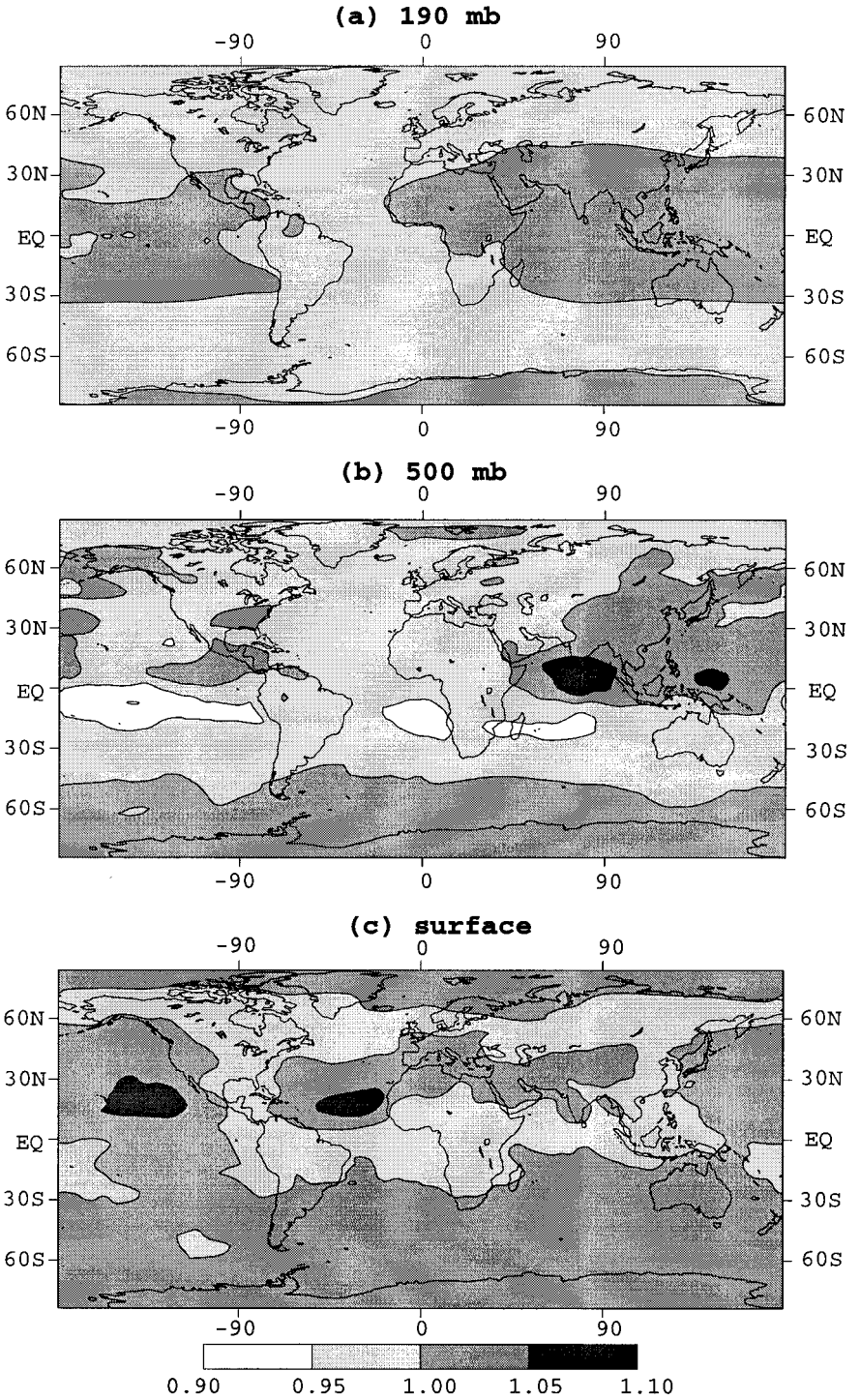

Figure 1. Monthly averaged ratios of July ozone fields obtained with the four-way look-up tables divided by the July ozone fields obtained with the fully equivalent operational model (FEOM) approximations for (a) 190 and (b) 500 mbar and (c) surface.

these two variables affect the chemical ozone production and destruction rates in an approximately linear manner.

On the basis of the coarse resolution specified in Table 6, only 320 box-model runs are required to construct a large FEOM for a given altitude, latitude, month, and surface type. The resultant computational efforts for constructing the whole set of large FEOMs are then reduced by a factor of 3 to ~0.9 million box-model runs. The grid resolutions in the small

Table 6. Coarse Grid Resolution of Large FEOMs

Input Variable	Range	Reference Point
Relative humidity	20%, 60%, 100%	60%
CO, ppb	50, 100, 200	100
NO_x, ppt	1, 50, 100, ⋯, 900, 950	450
Ozone, ppb	20, 40, ⋯, 180, 200	100

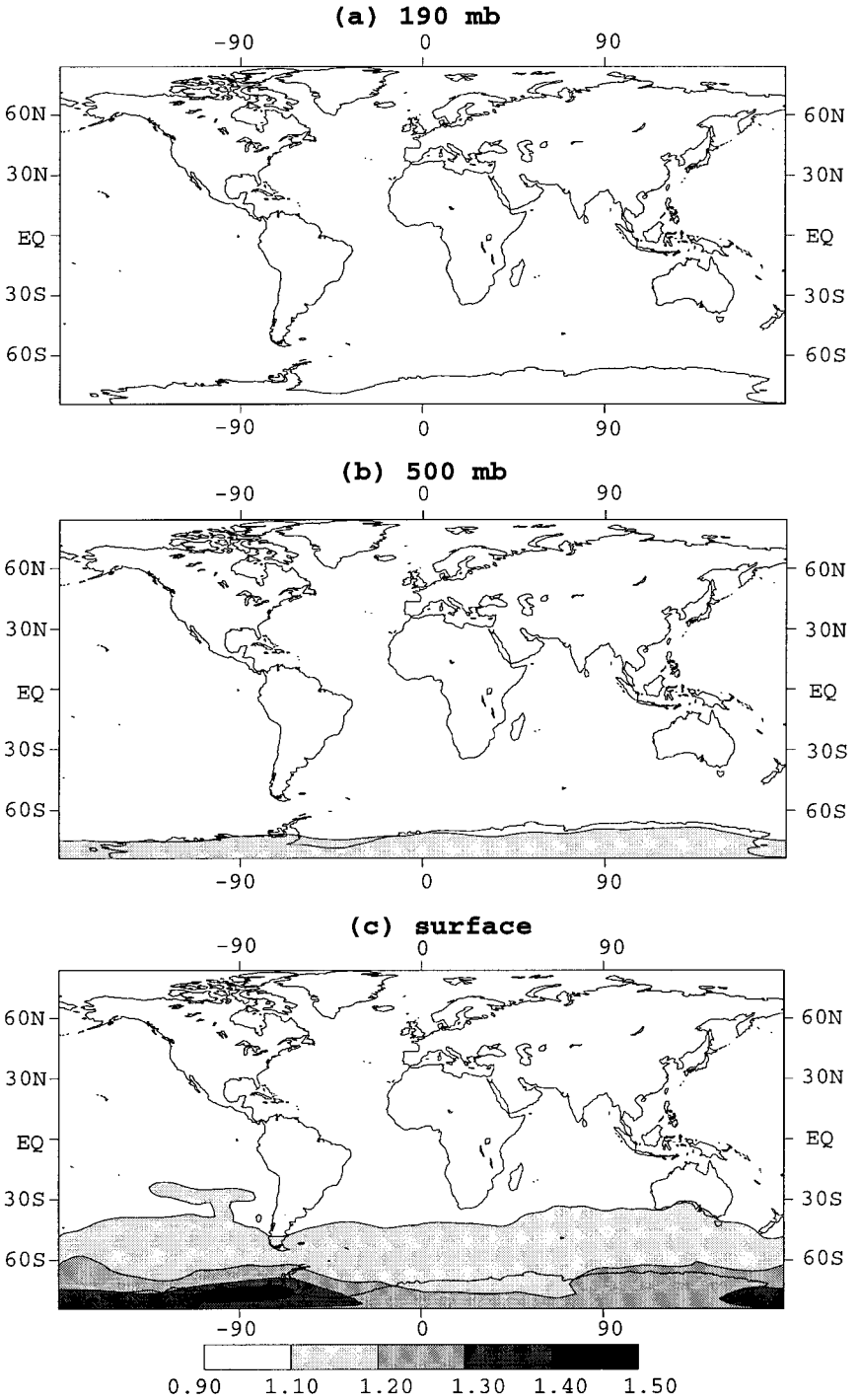

Figure 2. Monthly averaged ratios of February ozone fields obtained with the four-way look-up tables divided by the July ozone fields obtained with the FEOM approximations for (a) 190 and (b) 500 mbar and (c) surface.

FEOMs remained the same, since they call for negligible computational time. Comparing the global ozone fields between the fine resolution and the coarse resolution of the large FEOMs, the disagreements are within an acceptable $\pm 3\%$ across all levels of the troposphere.

4.3. Simulated Ozone Fields

The simulated global ozone fields over a period of 1 year, using the coarse scale FEOM, were compared with those obtained from the previous simulation [*Levy et al*., 1997; *Klonecki*, 1998], where the four-way interpolative look-up tables were used to obtain the chemical ozone production and destruction rates. Both sets of global ozone fields are generally in good agreement in the spring, summer, and autumn months. In the winter months, starting from December to March, higher disagreement (i.e., differences above 10%) appears in the region near the South Pole. Since similar patterns of disagreement occur for these four winter months, a comparison of the two

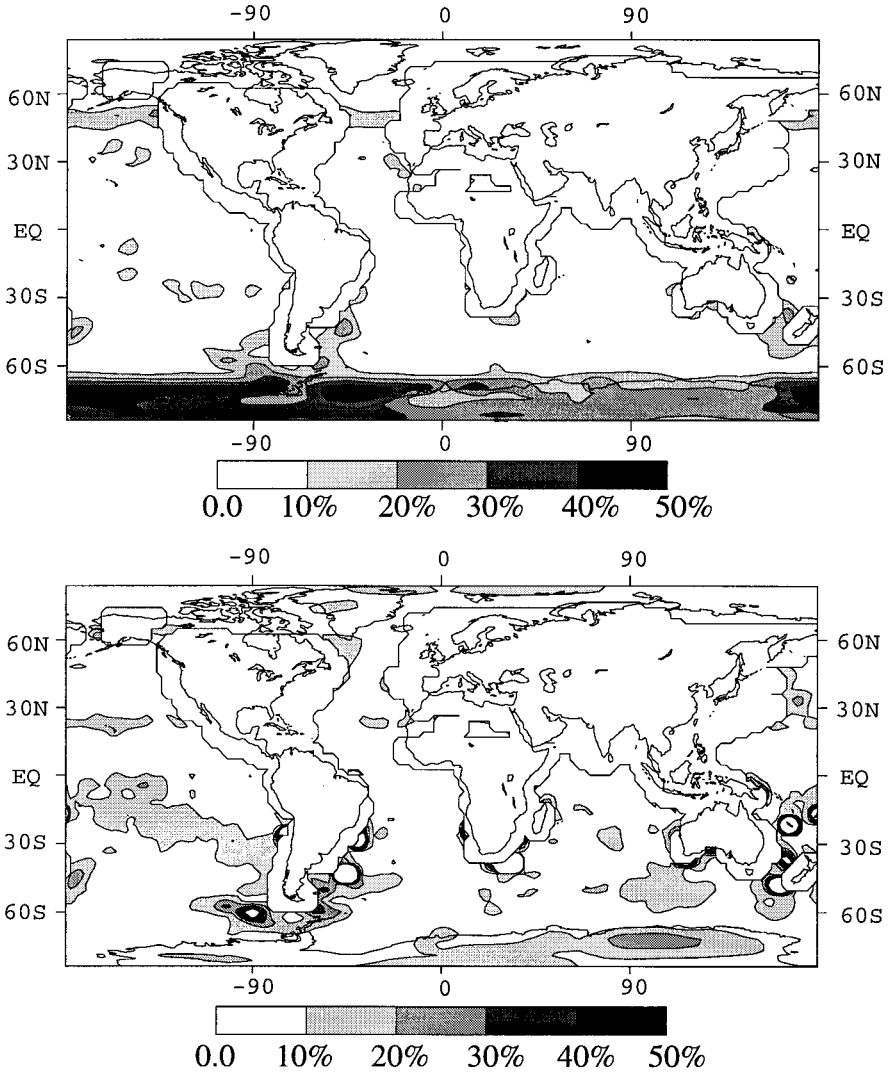

Figure 3. Percentage deviation from the exact solution of the ozone net chemical tendency predicted by the (top) four-way look-up table in the surface during February and (bottom) the FEOM approximation in the surface during February.

global ozone fields for February is shown in Figure 2 as representative of the four winter months.

In the upper troposphere (190 mbar), shown in Figure 2a, the two global ozone fields are in good agreement. The higher disagreement in the region near the South Pole gradually appears in the middle and lower troposphere, as shown in Figures 2b and 2c. The magnitude of the disagreement is highest value (50%) at the surface. To determine the origin of disagreement, the global fields of chemical ozone tendencies in February obtained from the two methods were compared with the "off-line" numerically exact solutions of box-model runs. The comparisons were performed by taking the monthly averaged values of the four input variables (H_2O, CO, NO_x, and O_3 concentrations) in each of the tropospheric grid boxes. As shown in Figure 3, there are about 30 to 50% deviations of the chemical ozone tendencies predicted by the four-way interpolative look-up tables around the area of the South Pole near the surface level, while the deviations of FEOMs predictions are generally within 10% in that area. This finding explains the high percentage differences between the ozone mixing ratio predictions from the two methods at the area near South Pole at low altitudes.

From the model performance evaluation in the previous simulation [*Levy et al*., 1997; *Klonecki*, 1998] the global ozone fields from the four-way interpolative look-up tables were generally in good agreement with the observed ozonesonde data, except at the two stations in the Antarctic region. The February ozone mixing ratios predicted from using FEOMs and the four-way interpolative look-up tables at these two stations as well as an island station are compared with the observations in Table 7. At the island station (Marambio), which is off the shore of the Antarctic, the simulated O_3 mixing ratios from both methods are generally in good agreement with the observation data. The simulated O_3 mixing ratios from the FEOMs and the four-way interpolative look-up tables are much too high compared to the observation data at the two stations (Syowa and South Pole) in the Antarctic. The ozone mixing ratios produced from the FEOMs are closer to the observations, due to the FEOM superior interpolation accuracy. Two additional sources of errors come from (1) the lack of simu-

Table 7. Model Performance Evaluation of O_3 Predictions

Station	Altitude	Observation	FEOMs	AAK*
Marambio	315 mbar	76.3 ppb	55.7 ppb	59.3 ppb
	500 mbar	26.5 ppb	25.7 ppb	27.3 ppb
	BL†	13.1 ppb	13.4 ppb	15.6 ppb
Syowa	315 mbar	74.0 ppb	77.4 ppb	80.0 ppb
	500 mbar	25.1 ppb	47.8 ppb	51.3 ppb
	BL†	18.2 ppb	22.7 ppb	26.1 ppb
South Pole	315 mbar	101.0 ppb	102.9 ppb	108.0 ppb
	500 mbar	24.5 ppb	51.5 ppb	60.7 ppb
	BL†	20.0 ppb	20.6 ppb	26.8 ppb

*AAK refers to the four-way look-up table.
†BL refers to the averaged value in the boundary layer.

lated stratospheric O_3 depletion leading to excessive levels of stratospheric O_3 available for transport into the troposphere over Antarctica and (2) the deficiencies in the simulated transport over Antarctica.

5. Conclusion

This paper demonstrated the feasibility of FEOMs as high-speed modules for chemical kinetics calculations in a 3-D GCTM study. The FEOMs are constructed by capturing the input-output behavior of chemical kinetics in correlated function expansions generated from a series of "off-line" photochemical box-model runs designed to capture the nonlinear tropospheric ozone chemistry in the CO-CH_4-NO_y-H_2O system. The resultant FEOMs are then used to predict the chemical ozone production and destruction rates based on the mixing ratios of the four tracers (O_3, NO_x, CO, and H_2O) in each of the tropospheric grid boxes during GCTM ozone simulations. The interpolated ozone production and destruction rates as well as the simulated global ozone fields using the FEOMs are more accurate than those obtained by the four-way interpolative look-up tables.

In constructing the FEOMs, special care is needed to ensure that the dynamic range for each of the input variables is properly covered. The computational run time using FEOMs in the GCTM simulation is comparable with the run time of using the four-way interpolative look-up tables for the present case study with four input variables. However, as the number of input variables increases, the advantage of using FEOMs will increase over that of the high-dimensional interpolative look-up tables, since the construction effort for high-dimensional look-up tables is prohibitive and the interpolation in high-dimensional space is more difficult. In another work on a stratospheric ozone box model there were 46 input variables, and the FEOM was at least $\sim 10^3$ faster than the original differential equation code with an overall error less than 3% [*Shorter et al*., 1999].

Although ~1 million box-model runs were required to construct the FEOMs, this effort is the one-time overhead for preparation of the FEOMs. No substantial computations are needed when employing the FEOMs in 3-D model simulations. As the number of input variables becomes sufficiently large, an efficient Monte Carlo sampling technique can be applied to generate the FEOMs [*Alis and Rabitz*, 1999]. Since 3-D GCTM simulations can call on a kinetic package ~1 billion times/year, the FEOM approach has the ability to relieve the computational burden and permit both multiple-year and multiple scenario simulations. Future work will focus on developing FEOMs for more complex and comprehensive atmospheric chemistry mechanisms, including nonmethane hydrocarbons.

Acknowledgments. The authors would like to thank A. Klonecki and W. Moxim for their assistance in carrying out this research. We would also like to thank J. Anderson and L. Donner for their careful reading of the manuscript and for their helpful comments. We acknowledge partial support from the New Jersey Department of Environmental Protection.

References

Alis, O. F., and H. Rabitz, Efficient implementation of high-dimensional model representations, in *Mathematical and Statistical Methods for Sensitivity Analysis*, edited by A. Saltelli, John Wiley, New York, in press, 1999.

Barnett, J. J., and M. Corney, Temperature data from satellites, in *The Middle Atmosphere Program Handbook*, vol. 16, pp. 3–11, 47–85, Spec. Comm. for Sol.-Terr. Phys., Secr., Univ. of Ill., Urbana, 1985.

DeMore, W. P., S. P. Sander, D. M. Golden, R. F. Hampson, M. J. Kurylo, C. J. Howard, A. R. Ravishankara, C. E. Kolb, and M. J. Molina, Chemical kinetics and photochemical data for use in stratospheric modeling, *JPL Publ*., *94–26*, 1994.

Kasibhatla, P. S., H. Levy II, A. A. Klonecki, and W. L. Chameides, A three-dimensional view of the large-scale tropospheric ozone distribution over the North Atlantic Ocean during summer, *J. Geophys. Res*., *101*, 29,305–29,316, 1996.

Kasibhatla, P. S., H. Levy II, and W. J. Moxim, Global NO_x, HNO_3, PAN, and NO distributions from fossil-fuel combustion emissions: A model study, *J. Geophys. Res*., *98*, 7165–7180, 1993.

Keating, G. M., M. C. Pitts, and D. F. Young, Ozone reference models for the middle atmosphere, *Adv. Space Res*., *10*(12), 317–355, 1990.

Klonecki, A. A., Model study of the tropospheric chemistry of ozone, Ph.D. thesis, Princeton Univ., N. J., 1998.

Klonecki, A. A., and H. Levy II, Tropospheric chemical ozone tendencies in CO-CH_4-NO_y-H_2O system: Their sensitivity to variations in environmental parameters and their application to a global chemistry transport model study, *J. Geophys. Res*., *102*, 21,221–21,237, 1997.

Komhyr, W. D., S. J. Oltmans, P. R. Franchois, W. F. J. Evans, and W. A. Matthews, The latitudinal distribution of ozone to 35 km altitude from ECC ozonesonde observations, 1985–1987, pp. 147–150, in *Ozone in the Atmosphere*, A. Deepak, Hampton, Va., 1989.

Levy, H., II, and W. J. Moxim, Simulated global distribution and deposition of reactive nitrogen emitted by fossil fuel combustion, *Tellus*, *41*, 256–271, 1989.

Levy, H., II, J. D. Mahlman, and W. J. Moxim, Tropospheric N_2O variability, *J. Geophys. Res*., *87*, 3061–3080, 1982.

Levy, H., II, P. S. Kasibhatla, and W. J. Moxim, A global three-dimensional time-dependent lightning source of tropospheric NO_x, *J. Geophys. Res*., *101*, 22,911–22,922, 1996.

Levy, H., II, P. S. Kasibhatla, W. J. Moxim, A. A. Klonecki, A. I. Hirsch, S. J. Oltmans, and W. L. Chameides, The global impact of human activity on tropospheric ozone, *Geophys. Res. Lett*., *24*, 791–794, 1997.

Levy, H., II, W. J. Moxim, A. A. Klonecki, and P. S. Kasibhatla, Simulated Tropospheric NO_x: Its evaluation, global distribution, and individual source contributions, *J. Geophys. Res*., in press, 1999.

Logan, J. A., Tropospheric ozone: Seasonal behavior, trends, and anthropogenic influence, *J. Geophys. Res*., *90*, 10,463–10,482, 1985.

Mahlman, J. D., and W. J. Moxim, Tracer simulation using a global general circulation model: Results from a mid-latitude instantaneous source experiment, *J. Atmos. Sci*., *35*, 1340–1374, 1978.

Manabe, S., D. G. Hahn, and J. L. Holloway, The seasonal variation of the tropical circulation as simulated by a global model of the atmosphere, *J. Atmos. Sci*., *31*, 43–83, 1974.

McKeen, S. A., et al., The photochemistry of acetone in the upper troposphere: A source of odd-hydrogen radicals, *Geophys. Res. Lett*., *24*, 3177–3180, 1997.

Meier, R. R., D. E. Anderson Jr., and M. Nicolet, Radiation field in the troposphere and stratosphere from 240–1000 nm, 1, General analysis, *Planet. Space Sci*., *30*, 923–931, 1982.

Moxim, W. J., H. Levy II, and P. S. Kasibhatla, Simulated global tropospheric PAN: Its transport and impact on NO_x, *J. Geophys. Res*., *101*, 12,621–12,638, 1996.

Orris, R. L., Ozone and temperature: A test of the consistency of

models and observations in the middle atmosphere, Ph.D. thesis, Princeton Univ., Princeton, N. J., 1997.

Perliski, L. M., The role of multiple scattering in twilight zenith sky observations of atmospheric absorbers: Diurnal photochemistry and airmass factors, Ph.D. thesis, Univ. of Colo., Boulder, 1992.

Rabitz, H., and K. Shim, Multicomponent semiconductor material discovery using a generalized correlated function expansion, *Phys. Rev*., *Ser. B*, in press, 1999.

Rabitz, H., and O. F. Alis, General foundation of high dimensional model representations, *J. Math. Chem*., *25*, 2–3, 1999.

Rabitz, H., O. F. Alis, J. Shorter, and K. Shim, Efficient input-output model representations, *Comput. Phys. Comm*., *115*, 1–10, 1998.

Shim, K., and H. Rabitz, Independent and correlated composition behavior of material properties: Application to energy band gaps for the $Ga_\alpha In_{1-\alpha} P_\beta As_{1-\beta}$ and $Ga_\alpha In_{1-\alpha} P_\beta Sb_\gamma As_{1-\beta-\gamma}$, *Phys. Rev. B Condens. Matter*, *58*, 1940–1946, 1998.

Shorter, J., P. C. Ip, and H. Rabitz, An efficient chemical kinetics solver using high dimensional model representation, *J. Phys. Chem. A*, *103*(36), 7192–7198, 1999.

Spivakovsky, C. M., S. C. Wofsy, and M. J. Prather, A numerical method for parameterization of atmospheric chemistry: Computation of tropospheric OH, *J. Geophys. Res*., *95*, 18,433–18,440, 1990a.

Spivakovsky, C. M., R. Yevich, J. A. Logan, S. C. Wofsy, and M. B. McElroy, Tropospheric OH in a three-dimensional chemical tracer model: As assessment based on observations of CH_3CCl_3, *J. Geophys. Res*., *95*, 18,441–18,471, 1990b.

Turanyi, T., Parameterization of reaction mechanisms using orthogonal polynomials, *Comput. Chem*., *18*(1), 45–54, 1994.

G. Li and H. Rabitz, Department of Chemistry, Princeton University, Princeton, NJ 08540.

H. Levy II, Geophysical Fluid Dynamics Laboratory, Princeton, NJ 08542.

S. Wang, NOAA/GFDL, P.O. Box 308, Princeton, NJ 08542. (sww@gfdl.gov)

(Received April 14, 1999; revised July 29, 1999;
accepted August 6, 1999.)